SYNTHESIS OF NEW CHITOSAN-CARBONATE HYDROXYAPATITE COMPOSITES WITH POTENTIAL APPLICATION IN BONE TISSUE ENGINEERING – PHYSICOCHEMICAL ANALYSIS

Justyna Urbaniak[1], Barbara Kołodziejska[2, a], Agnieszka Kaflak[3, b,*]

[1]Student scientific group 'Spectrum' Medical University of Warsaw, ul. Banacha 1, 02-097 Warsaw, Poland

[2]Department of Analytical Chemistry and Biomaterials, Medical University of Warsaw, ul. Banacha 1, 02-097 Warsaw, Poland
[a] - ORCID: 0000-0003-4325-8290

[3]Department of Analytical Chemistry and Biomaterials, Analytical Group, Medical University of Warsaw, ul. Banacha 1, 02-097 Warsaw, Poland
[b] - ORCID: 0000-0002-6864

** corresponding author: agnieszka.kaflak@wum.edu.pl*

Abstract

The subject of this study was the synthesis of 12 chitosan-hydroxyapatite (CH:HA) composites with different contents of carbonate ions (CO_3^{2-}), in two weight ratios of CH to HA (30:70 and 50:50), and two viscosities of CH (low [L] and high [H]). The method of direct co-precipitation of the introduced reagents was used. The structure of the obtained materials was characterised by Fourier-transform infrared (FT-IR) spectroscopy, powder X-ray diffraction, and scanning electron microscopy. The FT-IR spectra revealed the bands and ranges of the characteristic bands for CH and HA. The presence of CO_3^{2-} introduced into the structure of the obtained composites was identified by infrared spectroscopy. A reduction in the size of HA unit cells was observed in the obtained CH:HA biocomposites, in materials with a higher content of incorporated CO_3^{2-}. The obtained nanomaterials are similar to natural bone tissue. Future research will focus on the evaluation of the obtained materials as a drug delivery system.

Keywords: *chitosan, hydroxyapatite, biocomposite CH:HA, bone tissue, FT-IR, PXRD*

Received: 18.03.2022
Accepted: 30.06.2022

1. Introduction

Over the years, there has been a significant increase in human life expectancy [1]. With age, the bone mass decreases [2], and in addition, injuries, accidents, diseases, and tumours cause more and more people to suffer from problems with the skeletal system [3-5]. Like many tissues, bones can regenerate [6]. However, sometimes natural bone regeneration fails and some clinical interventions are required. Bone substitutes are increasingly used in surgery as over 2 million bone grafting procedures are performed worldwide annually. Autografts still represent the gold standard for bone substitution, although morbidity and the inherent limited availability are the main limitations [7]. Engineered bone tissue has been viewed as a potential alternative to conventional bone grafts due to their limitless supply and no disease transmission [8]. The implantation of synthetic bone-like materials is one of the safest treatment methods due to the limited possibilities of collecting biological material, reduced mortality risk, and induction of an immune response [5]. For the above-mentioned reasons, the search for biomimetic materials is currently one of the main goals of biomedical engineering [9, 10].

A wide variety of bone substitutes have been designed over the past 50 years [7]. Bone substitutes can be classified into two main categories: bone substitutes derived from biological products and synthetic bone substitutes [11]. Natural substitutes derived from biological products are: demineralised bone matrix (DBM); bone morphogenetic proteins (BMP); platelet-rich plasma; coral or natural calcium phosphate hydroxyapatite (HA) with the general formula $Ca_{10}(PO_4)_6(OH)_2$; and synthetic bone-like products including calcium sulphate, calcium phosphate cement (CPCs), bioactive glasses, and two-phase calcium phosphates, including polymers that can be divided into natural and natural synthesised biopolymers [7, 12]. Natural biopolymers include collagen and chitosan (CH) materials, silk polymers, gelatine scaffolds, and alginate composites. Artificial biopolymers include polyethylene materials, composites based on polylactic acid (PLA), polyether ketones (PEEK), copolymers of lactic, and poly(lactic-co-glycolic) acid (PGLA) [11]. Regardless of the material used, all bone substitutes should reflect the natural structure of bone with a porous surface that promotes mucoadhesion and activates osteoblasts. They should be biocompatible with the natural bone tissue, biodegradable, and have adequate mechanical strength [11].

Among implant materials, HA materials have the highest biocompatibility [6, 13]. Additionally, they do not cause an inflammatory response, and a porosity of 65% in the cancellous bone provides osteoinductive properties [12, 14]. Despite numerous superlatives, HA itself has low mechanical strength, a low rate of bonding with the host bone tissue, and a long resorption time, which may hinder the process of osseointegration and cause slow progression of bone ingrowth and cell colonisation [12, 14, 15].

CH is a deacetylated form of chitin, which is synthesised by different crustaceans, molluscs, marine diatoms, insects, algae, fungi, and yeasts [16-18]. The polymer belongs to the crystalline polysaccharides and is composed of β (1 → 4)-D-glucosamine and *N*-acetyl-D-glucosamine subunits, arranged randomly or in blocks in the structure of the polymer chain [19]. CH exhibits properties desirable for biomaterials because it is biocompatible, biodegradable, hydrophilic, and non-toxic. Its porous structure facilitates penetration and binding with other cells, especially bone cells [20].

Developing a composite containing HA and CH improves the mechanical properties of both components. The obtained material has a greater resistance to compression, and the process of biological tissue reconstruction is accelerated [21]. Additionally, the material obtained in this way is completely non-toxic, non-immunogenic, non-inflammatory, and characterised by a high degree of biocompatibility and osteoinductivity [21-24].

CH-HA composites can be prepared using various synthetic methods for example, single-stage co-precipitation [13, 25-29], hydrothermal [30-34], solid-phase reaction [34, 35], and sol-emulsion gel [10, 36, 37]. The co-precipitation method, otherwise known as the wet method, has many advantages, such as: the speed of producing a large amount of product, easy control of particle size, low cost, and unlimited possibilities to modify the overall homogeneity of the product [38].

It is also necessary to focus on the carbonate ion (CO_3^{2-}) content in the bone tissue mineral. It is estimated that these ions comprise 6%-9% of bone tissue, and they can be incorporated into the structure of HA in the positions of orthophosphate anions (type B apatite), hydroxyl anions (type A apatite), or both at the same time (mixed type AB apatite) [39]. The presence of CO_3^{2-} reduces the size of HA crystals, which increases the reactivity of bone apatites, which in turn leads to the acceleration of resorption processes, increased biomimeticity, and faster treatment time [6, 40, 41]. The study aimed to develop an effective method of synthesis of CH:HA composites enriched with CO_3^{2-} with the desired physicochemical and biological properties as potential biomaterials in bone tissue engineering.

2. Materials and Methods

2.1. Synthesis of CH:HA Composites

The synthesis was based on the direct co-precipitation method to obtain two CH:HA composites with the ratios of 30:70 and 50:50, with the addition of 2, 1, or 0 moles of CO_3^{2-} in relation to the structure of HA ($Ca_8(PO_4)_4(CO_3)_2$) molecule, using low-viscosity (L) and high-viscosity (H) CH.

2.2. Direct Co-precipitation Method

Low-viscosity CH from shrimp shells and high-viscosity CH from crab shells were dissolved in 1% acetic acid solution to obtain a CH concentration of 0.2% (*w/v*). The solution was mixed vigorously with a magnetic stirrer until the CH was completely dissolved. Then, aqueous solutions of 1.0 mol dm^3 Calcium nitrate tetrahydrate ($Ca(NO_3)_2$) and 1.0 mol/dm^3 ammonium phosphate dibasic (Na_2HPO_4) for high-performance liquid chromatography were added to maintain the calcium-to-phosphorus ratio at 1.67; 1.0 mol/dm^3 solution ammonium carbonate (NH_4CO_3) analytical grade was also added. With constant stirring, the reaction medium was made alkaline with 25% ammonia solution to pH 11 and stirred until complete precipitation. The obtained products were matured for 7 days at 25°C, 1013 hPa, with access to daylight. Then, the precipitate was centrifuged (3500 rpm, 4 min) and washed with deionised water until a solution over the precipitate obtained a neutral pH. After freezing in dry ice (for 40 min), the obtained composites (Table 1) were subjected to 72 hours of lyophilisation (reduced temperature and pressure of 0.12 mBar).

Table 1. Characteristics of 12 chitosan-hydroxyapatite (CH:HA) composites.

CH:HA	**30:70**						**50:50**					
Moles of CO_3^{2-}	0	1	2	0	1	2	0	1	2	0	1	2
CH viscosity	Low			High			Low			High		
Name	1L0	1L1	1L2	1H0	1H1	1H2	2L0	2L1	2L2	2H0	2H1	2H2

2.3. Physicochemical Methods to Analyse the Obtained Composites

The obtained materials were subjected to physicochemical analysis using Fourier-transform infrared (FT-IR) spectroscopy, X-ray powder diffraction (PXRD), and scanning electron microscopy (SEM). The FT-IR spectroscopic measurements were performed using the potassium bromide tablet method (FT-IR Spectrum 1000 by Perkin Elmer coupled with a computer) and the attenuated total reflectance method (ATR; Shimadzu FT IR IRAffinity-1S spectrometer). FT-IR spectra were recorded in the range 4000-400 cm^{-1} (for both techniques). In the classic IR method, tablets were prepared by mixing approximately 200-220 mg of potassium bromide with 1-2 mg of a sample of the obtained composite and compressing them (at 10 tons) to form a tablet. All FT-IR spectra were developed with GRAMS software/Al 8.0 (Thermo Scientific).

A JEOL JSM 6390 LV scanning electron microscope was used for SEM at 20 or 30 kV accelerating voltage. P-XRD measurements of the HAP and fluoride-substituted materials were performed using a Bruker D8 Advance diffractometer. The measurements were carried out using CuKa radiation ($\lambda = 1.54$ Å) over the 2θ range of 10-80°, using a step size of 0.03°. For crystallite size estimation, we calculated the full width at half maximum for the reflection of the (002) and (300) planes, representing the crystallites along the c-axis and a-axis, respectively. The Scherrer formula was used [42].

3. Results and Discussion

Table 1 provides details on the 12 synthesised CH:HA composites, with two organic-to-inorganic fractions (30:70 and 50:50).

Scanning electron micrographs of the obtained CH:HA composites are shown in Figures 1 and 2, highlighting differences in morphology. Composites obtained with low-viscosity CH (1L-2L) form heterogeneous agglomerates with a dense structure and a rough, ragged surface. This type of surface promotes the bioadhesion of bone cells and thus bone regeneration [20]. No agglomerates are visible in scanning electron micrographs of composites obtained with high-viscosity CH. They are characterised by high porosity, a thread-like structure and a less rough surface than composites obtained with low-viscosity CH. Porosity ensures good vascularisation and thus the supply of essential nutrients to the damaged tissue [20], which may result in greater resorption and thus the acceleration of bone tissue regeneration processes.

The difference in the content of the organic fraction among the synthesised composites may affect their structure depending on the viscosity of CH. Scanning electron micrographs of composites containing low-viscosity CH and a higher ratio of CH:HA (2L0-2L2) have a more porous structure than materials obtained from high-viscosity CH and a higher ratio of CH:HA (1H0-2H2). The latter is characterised by a less 'rough' surface than composites with a higher content of an inorganic fraction (1H0-2H2 and 2H0-2H2). Scanning electron micrographs revealed no significant differences in the structure of composites containing the addition of CO_3^{2-} (compare 1/2H1-2 and 1/2L1-2).

PXRD of the synthesised CH:HA composites revealed differences between individual materials in the intensity and width of the reflections in the obtained diffraction patterns. When there was inorganic content in the composite, the obtained diffraction pattern showed better separation of reflections and their relative intensity increased. The obtained results of the crystal sizes are presented in Table 2. It is noteworthy that the introduction of CO_3^{2-} into the HA structure in the synthesised composites significantly reduced the crystal length in relation to the *c*-axis (Table 2). Surprisingly, the 2L0-2L2 materials did not show this tendency, a phenomenon that requires further testing or repeated synthesis. The reduction in the unit cell parameter (e.g., the length in relation to the *c*-axis) after the introduction of CO_3^{2-} into the HA structure destroys/shortens the parameters of the HA unit cell, a finding consistent with previous reports [43, 44].

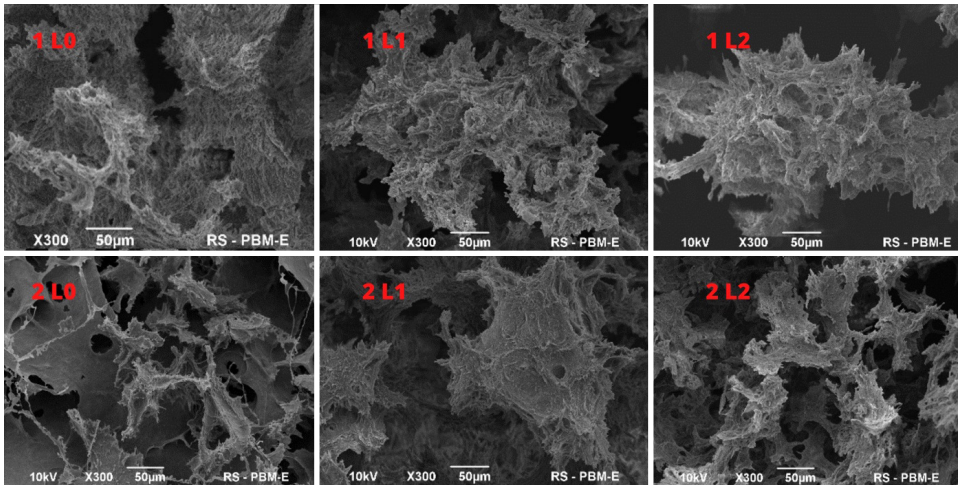

Figure 1. Scanning electron micrographs of composites containing low-viscosity chitosan (1L0-2L2).

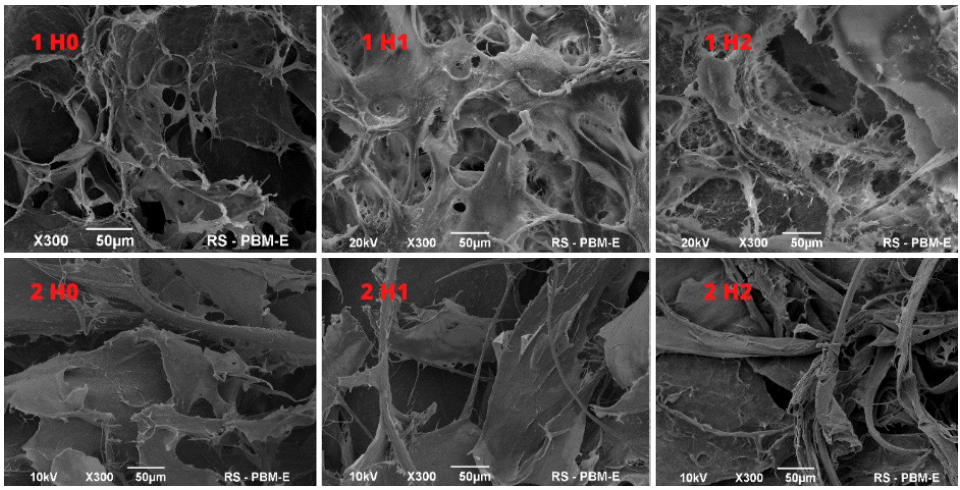

Figure 2. Scanning electron micrographs of composites containing high-viscosity chitosan (1H0-2H2).

Table 2. Parameters obtained from X-ray powder diffraction data.

CH:HA	Sample ID	Crystal size *c*-axis [002] [nm]
30:70	1**H**0	18.47
	1**H**1	13.01
	1**H**2	10.48
	1**L**0	16.38
	1**L**1	11.87
	1**L**2	-
50:50	2**H**0	15.87
	2**H**1	10.50
	2**H**2	11.92
	2**L**0	16.92
	2**L**1	15.55
	2**L**2	16.57

Table 3. Characteristic bands from the Fourier-transform infrared spectra.

CH viscosity	**Low**		**High**		**Low**		**High**	
CH:HA	**30:70**	**50:50**	**30:70**	**50:50**	**30:70**	**50:50**	**30:70**	**50:50**
Band and type of vibrations	**FT-IR ATR**				**FT-IR (KBr tablet)**			
	Wavenumber [cm^{-1}]							
ν OH/ N-H	3366		3360		3440			
ν C-H	2280		2910 -*	2930 2890	2920 2860	2930 2880	2920 2870	2930 2870
ν C=O (amid I)	1650	1650	1650	-*	1650	1660	1660	
δ H_2O	-*	1640	-*	1640	-*		1640	
ν_2 CO_3^{2-}	1490		1490	-*	1490	-*	1495	-*
δ C-H/ CO_3^{2-}	1421	1424	1420		1420			1427
ν C-N (amid III)	-*	-*	-*	-*	1380 1320		-* 1310	1380 1320
ν_3, ν_1 symmetric/ asymmetric PO_4^{3-}	-*	-*	1140		1110	1100	1114	1100
	1024		1020		1030		1026	
ν_2 CO_3^{2-}	875		870		870	860	869	
δ OH	-*	-*	-*	-*	670	660	-*	664
ν_4 PO_4^{3-}	602 558		600 560		600 560		605 566	605 556

* - not present in the the Fourier-transform infrared spectra

The obtained FT-IR spectra of CH:HA composites revealed characteristic bands from both the organic (CH) and inorganic (HA) fractions (Table 3 and Figures 3 and 4). FT-IR spectra obtained with the ATR technique analyse the surface of the tested material, while the spectra obtained with the KBr tablet technique reflect the entire analysed material (averaging the scratchiness from both the inside and the surface of the tested composite). The obtained spectra present four areas with bands. The first and second are intense bands in the range of 1150-900 cm^{-1} and 650-500 cm^{-1}, which correspond to the stretching and bending vibrations of the phosphate groups in the HA structure [45]. There are also P=O stretching vibrations in the range of 1350-1150 cm^{-1}. The broadening of the bands

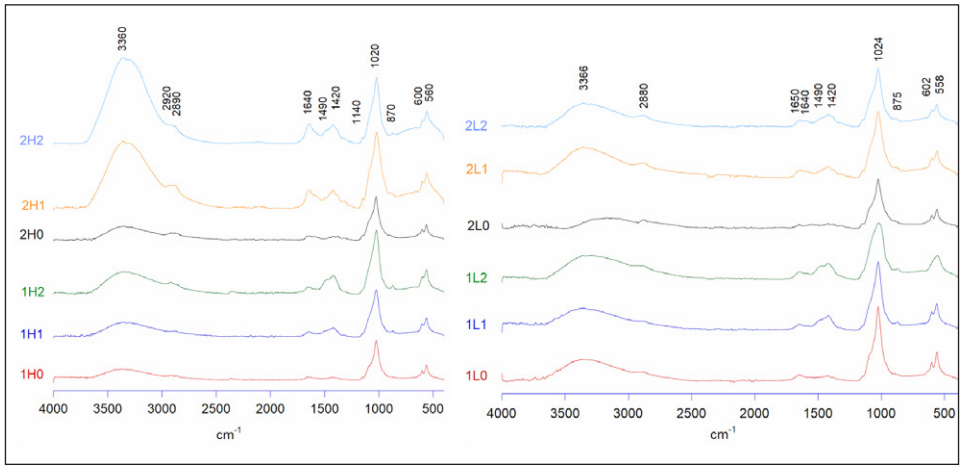

Figure 3. Fourier-transform infrared spectra of the materials obtained with high-viscosity (on the left) and low-viscosity chitosan (on the right) (using the attenuated total reflectance method).

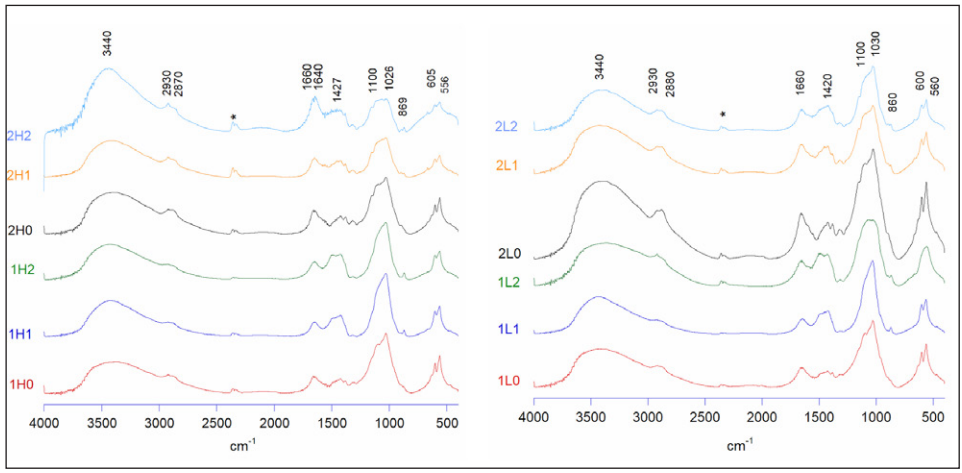

Figure 4. Fourier-transform infrared spectra of the materials obtained with high-viscosity (on the left) and low-viscosity (on the right) chitosan (KBr tablet).

in the range of 1240-900 cm^{-1} may indicate the interaction of HA with CH.

In the region of 1660-1250 cm^{-1}, there are mainly bands originating from CH. In this range, the bands of stretching vibrations of the C=O groups (νC=O, approximately 1650 cm^{-1}) and CH

bending vibrations (δCH, approximately 1420 cm^{-1}) can be distinguished. The higher the content of the composite's organic fraction, the higher the intensity of the bands in this area (compared materials 2L, 2H with materials 1L, 1H, Figures 3 and 4). It is also worth noting that in this area at 1420 and 1460 cm^{-1}, there should be visible bands originating from CO_3^{2-} introduced into the synthesised material. The band at about 1420 cm^{-1} can be distinguished, although its intensity 'covered' by the organic fraction present in the obtained composites may be difficult to identify/interpret.

In the area above 2800 cm^{-1}, there is a wide band originating from water molecules on the slope of which there are bands resulting from vibrations from -CH stretching at 2880 and 2930 cm^{-1}. The intensity of these bands increases as the CH content in the composites increases [26, 46]. Composites containing CO_3^{2-} (1H1, 1H2, 1L1, 1L2, 2H1, 2H2, 2L1, and 2L2, Figure 4) show a faintly outlined band in the range of $n_2CO_3^{2-}$ (at 875 cm^{-1}) corresponding to the asymmetric vibrations of CO_3^{2-}. Its weak intensity may result from a relatively small amount of CO_3^{2-} ions built into the structure of the composite [10, 46, 47].

4. Conclusions

During the research, a series of CH:HA composites were synthesised in two molar ratios of the organic and inorganic fraction, that is, HA with incorporated CO_3^{2-}. The physicochemical analysis of the obtained biocomposites with FTIR, PXRD, and SEM revealed differences in the morphology, intensity, and width of reflections, or the intensity and width of bands in spectra. There is a visible relationship between the viscosity of the CH used and the agglomeration of its particles, as well as the CH:HA ratio and the porosity of the structure. X-ray analysis showed that the introduction of CO_3^{2-} into the structure of HA in the synthesised composites causes a significant reduction in the HA unit cell parameter in the composites. The presence of CO_3^{2-} in the obtained nanocomposites was confirmed by bands in FT-IR spectra (low intensity). The obtained composites could probably be used as biomaterials to release the active substance in bone defect engineering.

5. Acknowledgments

This work was supported by the Medical University of Warsaw.

6. References

[1] GBD; (2015) Global, regional, and national age–sex specific all-cause and cause-specific mortality for 240 causes of death, 1990–2013: a systematic analysis for the Global Burden of Disease Study. Lancet 385, 117-71.

[2] Chan GK, Duque G; (2002) Age-related bone loss: old bone, new facts. Gerontology 48, 62-71. **DOI**:10.1159/000048929

[3] Siddiqui HA, Pickering KL, Mucalo MR; (2018) A review on the use of hydroxyapatite-carbonaceous structure composites in bone replacement materials for strengthening purposes. Materials, 11, 1813. **DOI**:10.3390/ma11101813

[4] Murugan R, Ramakrishna S; (2004) Bioresorbable composite bone paste using polysaccharide based nano hydroxyapatite. Biomaterials Vol. 25, 3829–3835. **DOI**:10.1016/j.biomaterials.2003.10.016

[5] Swetha M, Sahithi K, Moorthi A, Srinivasan N, Ramasamy K, Selvamurugan K; (2010) Biocomposites containing natural polymers and hydroxyapatite for bone tissue engineering. Int J Biol Macromol 1, 1-4. **DOI**:10.1016/j.ijbiomac.2010.03.015

[6] Kashirina A, Yao Y, Liu Y, Leng J; (2019) Biopolymers for bone substitutes: a review. Biomater Sci 10, 3961-3983. **DOI**:10.1039/c9bm00664h

[7] Campana V, Milano G, Pagano E, Barba M, Cicione C, Salonna G, Lattanzi W, Logroscino W; (2014) Bone substitutes in orthopaedic surgery: from basic science to clinical practice. J Mater Sci, Mater Med 25: 2445-2461. **DOI**:10.1007/s10856-014-5240-2

[8] Amini AR, Laurencin CT, Nukavarapu SP; (2012) Bone tissue engineering: recent advances and challenges. Crit Rev Biomed Eng 40(5):363-408. **DOI**:10.1615/critrevbiomedeng.v40.i5.10

[9] Mallick K; (2014) Bone substitute biomaterials, Elsevier, Cambridge.
[10] Brahimi S, Ressler A, Boumchedda K, Hamidouche M, Kenzour A, Djafar R, Antunović M, Bauer L, Hvizdoš P, Ivanković H; (2022) Preparation and characterization of biocomposites based on chitosan and biomimetic hydroxyapatite derived from natural phosphate rocks. Mat Chem Phys, 276, 125421. **DOI**:10.1016/j.matchemphys.2021.125421
[11] Fernandez de Grado G, Keller L, Idoux-Gillet Y, Wagner Q, Musset A, Benkirane-Jessel N, Bornert F, Offner D; (2018) Bone substitutes: a review of their characteristics, clinical use, and perspectives for large bone defects management. J Tissue Eng. 9, 1-18. **DOI**:10.1177/2041731418776819
[12] Sobczak A, Kowalski Z; (2007) Materiały Hydroksyapatytowe stosowane w implantologii. Czas Tech, Wydawnictwo PK, 149-158.
[13] Szatkowski T, Kołodziejczak-Radzimska A, Zdarta J, Szwarc-Rzepka K, Paukszta D, Wyskokowski M, Ehrlich H, Jesionowski T; (2015) Synthesis and characterization of hydroxyapatite/chitosan composites. Physicochem Probl Miner Process 51, 575-585. **DOI**:10.5277/ppmp150217
[14] Daculsi G; (1998) Biphasic calcium phosphate concept applied to artificial bone, implant coating and injectable bone substitute. Biomaterials 19, 1473-1478. **DOI**:10.1016/s0142-9612(98)00061-1
[15] Koshino T, Murase T, Takagi T, Saito T; (2001) New bone formation around porous hydroxyapatite wedge implanted in opening wedge high tibial osteotomy in patients with osteoarthritis. Biomaterials 22, 1579-1582. **DOI**:10.1016/s0142-9612(00)00318-5
[16] Synowiecki J, Al-Khateeb NA; (2003) Production, properties, and some new applications of chitin and its derivatives. Crit Rev Food Sci Nutr 43, 145-171.
[17] Klinger C, Żółtowska-Aksamitowska S, Wysokowski M, Tsurkan MV, Galli R, Petrenko I, Machałowski T, Ereskovsky A, Martinović R, Muzychka L, Smolii O, Bechmann N, Ivanenko V, Schupp P, Jesionowski T, Giovine M, Joseph Y, Bornstein S, Voronkina A, Ehrlich H; (2019). Express Method for Isolation of Ready-to-Use 3D Chitin Scaffolds from Aplysinaarcheri (Aplysineidae: Verongiida) Demosponge. Marine Drugs 17, 131. **DOI**:10.3390/md1702013
[18] Fadlaoui S, El Asri O, Mohammed L, Sihame A, Omari A, Melhaoui M; (2019) Isolation and characterization of chitin from shells of the freshwater crab Potamon algeriense. Prog Chem Appl Chitin Deriv 24, 23-35. **DOI**:10.15259/PCACD.24.002
[19] Szurkowska K, Zgadzaj A, Kuras M, Kolmas J; (2018) Novel hybrid material based on Mg^{2+} and SiO_4^{4-} co-substituted nano-hydroxyapatite, alginate and chondroitin sulphate for potential use in biomaterials engineering. Ceram Int 44, 18551-18559. **DOI**:10.1016/J.CERAMINT.2018.07.077
[20] Tolaimate A, Desbrie'res J, Rhazi M, Alagui A, Vincendon M, Vottero P; (2000) On the influence of deacetylation process on the physicochemical characteristics of chitosan from squid chitin. Polymer 41, 2463-2469. **DOI**:10.1016/S0032-3861(99)00400-0
[21] Ripamonti U, Roden LC, Renton LF; (2012) Osteoinductive hydroxyapatite-coated titanium implants. Biomaterials 33, 3813-3823. **DOI**:10.1016/j.biomaterials. 2012.01.050
[22] Rupani A, Bastida LAH, Rutten F, Dent A, Turner I, Cartmell S, (2012) Osteoblast activity on carbonated hydroxyapatite. J Biomed Mater Res. Part A 100, 1089-1096. **DOI**:10.1002/jbm.a.34037
[23] Jin HH, Kim DH, Kim TW, Shin KK, Jung JS, Parka HC, Yoon SY; (2012) In vivo evaluation of porous hydroxyapatite/chitosan–alginate composite scaffolds for bone tissue engineering. Int J Biol Macromol 51, 1079-1085. **DOI**:10.1016/j.ijbiomac.2012.08.027

[24] Bose S, Tarafder S; (2012) Calcium phosphate ceramic systems in growth factor and drug delivery for bone tissue engineering: a review. Acta Biomater 8(4), 1401-1421. **DOI**:10.1016/j.actbio.2011.11.017
[25] Lakrat M, Fadlaoui S, Aaddouz M, El Asri O, Melhaoui M, Mejdoubi EM; (2020) Synthesis and characterization of composites based on hydroxyapatite nanoparticles and chitosan extracted from shells of the freshwater crab Potamon algeriense. Prog Chem Appl Chitin Deriv 14, 23-35. **DOI**:10.15259/PCACD.24.002
[26] Danilchenko SM, Kalinkevich OV, Pogorelov MV; (2009) Chitosan–hydroxyapatite composite biomaterials made by a one step co-precipitation method: preparation, characterization and in vivo tests. Biol Phys Chem 9, 119-126. **DOI**:10.4024/22DA09A.JBPC.09.03
[27] Kong L, Gao Y, Cao W, Gong Y, Zhao N, Zhang X, (2005); Preparation and characterization of nano-hydroxyapatite/chitosan composite scaffolds. J Biomed Mater Res 75A, 275-282. **DOI**:10.1002/jbm.a.30414
[28] Li J, Chen YP, Yin Y, Yao F, Yao K; (2007) Modulation of nano-hydroxyapatite size via formation on chitosan-gelatin network film in situ. Biomaterials 28, 781-790. **DOI**:10.1016/j.biomaterials.2006.09.042
[29] Sarig S, Kahana F; (2002) Rapid formation of nanocrystalline apatite. J Cryst Growth 237-239, 55-59. **DOI**:10.1016/S0022-0248(01)01850-4
[30] Stępniewski M, Martynkiewicz J, Gosk J; (2017) Chitosan and its composites: properties for use in bone substitution. Polym Med 47, 49-53. **DOI**:10.17219/pim/76517
[31] Earl JS, Wood DJ, Milne SJ; (2006) Hydrothermal synthesis of hydroxyapatite. J Phys Conf Ser. 26, 268-271. **DOI**:10.1088/1742-6596/26/1/064
[32] Kothapalli CR, Wei M, Legeros RZ, Shaw MT; (2005) Synthesized by the hydrothermal method. J Mater Sci Mater Med 16, 441-446. **DOI**:10.1007/s10856-005-6984-85
[33] Cihlar J, Castkova K; (2002) Direct synthesis of nanocrystalline hydroxyapatite by hydrothermal hydrolysis of alkylphosphates. Chem Mon 133, 761-771. **DOI**:10.1007/s00706020004
[34] Liu J, Ye X, Wang H, Zhu M, Wang B, Yan H; (2003) The influence of pH and temperature on the morphology of hydroxyapatite synthesized by hydrothermal method. Ceram Int 29, 629-633. **DOI**:10.1016/S0272-8842(02)00210-9
[35] Du X, Chu Y, Xing S, Dong L; (2009) Hydrothermal synthesis of calcium hydroxyapatite nanorods in the presence of PVP. J Mater Sci 44, 6273-6279. **DOI**:10.1007/s10853-009-3860-6
[36] Rao RR, Roopa HN, Kannan TS; (1997) Solid state synthesis and thermal stability of HAP and HAP-beta-TCP composite ceramic powders. J Mater Sci Mater Med 8, 511-518. **DOI**:10.1023/a:1018586412270
[37] Vijayalakshmi U, Rajeswari S; (2012) Influence of process parameters on the sol-gel synthesis of nanohydroxyapatite using various phosphorus precursors. J Sol Gel Sci Technol. 63, 45-55. **DOI**:10.1007/s10971-012-2762-2
[38] Jillavenkatesa A, Condrate RA (1998) Sol-gel processing of hydroxyapatite. J Mater Sci 33, 4111-4119. **DOI**:10.1023/A:1004436732282
[39] Boudemagh D, Venturini P, Fleutot S, Cleymand F; (2019) Elaboration of hydroxyapatite nanoparticles and chitosan/hydroxyapatite composites: a present status. Polym Bull. 76, 2621-2653. **DOI**:10.1007/s00289-018-2483-y
[40] Błażewicz S, Stoch L; (2003) Biocybernetyka i inżynieria biomedyczna 2000, t.4, Biomateriały, AOW EXIT, Warszawa.

[41] Mc Lean FC, Budy AM; (1959) Connective and supporting tissues: bone. Annu Rev Physol 21, 69-90.

[42] Venkateswarlu, K; (2010) Bose, A.C.; Rameshbabu, N. X-ray peak broadening studies of nanocrystalline hydroxyapatite by Williamson–Hall analysis. Phys B Condens Matter. 405, 4256-4261. **DOI**:10.1016%2Fj.physb.2010.07.020

[43] Suparova M; (2015) Substituted hydroxyapatites for biomedical applications: a review. J Ceram Int 41, 9203-9231. **DOI**:10.1016/j.ceramint.2015.03.316

[44] Kaflak A, Kolodziejski W; (2011) Complementary information on water and hydroxyl groups in nanocrystalline carbonated hydroxyapatites from TGA, NMR and IR measurements. J Mol Struct 990, 263-270. **DOI**:10.1016/j.mol.struc.2011.01.056

[45] Dorozhkin SV; (2015) Calcium orthophosphate deposits: Preparation, properties and biomedical applications. Mater Sci Eng C Mater Biol Appl 55, 272-326. **DOI**:10.1016/j.msec.2015.05.033

[46] Ducheyne P, Helly K, Hutmacher D, Grainger D, Kirkpatrick C; (2011) Comprehensive biomaterials, 1st edn, Elsevier, Amsterdam.

[47] Trinkunaite-Felsen J, Stankeviciute Z, Yang JC, Yang TCK, Beganskiene A, Kareiva A; (2014) Calcium hydroxyapatite/whitlockite obtained from dairy products: simple, environmentally benign and green preparation technology. Ceram Int 40, 12717-12722. **DOI**:10.1016/j.ceramint.2014.04.120